A Correlation for Laminar, Low-Temperature, Gradient Heat and Mass Transfer Applied to a Low-Slope Roof

William A. Miller[1], Ph.D., P.E. **Jerald A. Atchley**
Member ASHRAE

ABSTRACT

An energy balance at the exterior surface of a roof is an essential boundary condition for mathematically describing the heat flow through a multilayered insulated roof. The dominant parameters affecting the heat flow during the daylight hours are convection and the surface properties of reflectance and emittance. At night and during the twilight hours, the infrared emittance and mass transfer balance against the roof's heat flow. The mass-transfer coefficient is calculated directly from a dimensionless term called the Lewis number and the air-side convective-heat-transfer coefficient. The approach is applicable to turbulent and laminar flow regimes. However, research has shown the calculation procedure questionable at both low velocities and small air-to-water temperature differences; conditions prevalent during the evening hours on a low-slope roof. Hence, a correlation was formulated and validated against experimental data to better estimate the mass-transfer coefficient and, therefore, the heat transfer through the roof when condensation or evaporation occurs.

INTRODUCTION

Large, open floor areas on one level characterize the industrial and commercial buildings of today. These single-story buildings have a large ratio of exposed exterior surface-to-floor area, and the roof is roughly 85% of the exposed exterior (Baker 1980). The roof has a very gradual slope of about 1.2° for the drainage of precipitation; this is typical of commercial roofing. The gradual slope allows the placement of mechanical and air-conditioning equipment, which saves the building owner useful floor space. Historically, the roof is built up with multiple layers of a felt paper applied to several applications of bitumen. Such roofs, called built-up roofs (BURs) offer excellent waterproofing and provide a service life of up to 20 years. However, the roof is the major source of heat leakage because of its large, exposed surface area and dark, heat-absorptive characteristic coupled with the demand for comfort cooling within the building.

In the summer, the higher the roof temperature, the greater the potential for heat leakage into a building, and the greater the burden on the air-conditioning system. For example, the exterior daytime temperature of a BUR can exceed 180°F (82°C) in predominantly hot climates. The temperature is strongly dependent on the roof's surface properties of reflectance (ρ) and emittance (ε). Convection ($\hbar$) is also important. When a roof's exterior temperature falls below the ambient air's dew point temperature, moisture condenses. The mass transfer also affects the temperature and heat transfer through the roof.

Mass transfer to a low-slope roof is very similar to the classical problem of forced-convection flow over a flat plate; it can be modeled using the well-established analogy between heat and mass transfer.

[1] **Dr. William A. Miller is a research engineer in the Buildings Technology Center of Oak Ridge National Laboratory (ORNL), Oak Ridge, Tennessee. Jerald Atchley is a technician working in support of ORNL's Building Thermal Envelope Systems & Materials Program.**

NOMENCLATURE

The following list contains various symbols and nomenclature used herein.

α	thermal diffusivity	$\overline{\rho}$	density
D_{ab}	mass diffusivity	ρ	total solar reflectance
Ca	concentration of moist air	σ	Stefan-Boltzmann constant
C_P	specific heat	x	dimension in plane of roof
$\hbar$	convection coefficient	z	dimension perpendicular to roof
h_m	mass-transfer coefficient	**Subscript**	
I	solar radiation	air	humid air
i	enthalpy	atm	atmosphere
i_{fg}	latent heat of water vapor	b	interior control volume boundary
k	thermal conductivity	c	transition to turbulence
L	length in x-direction of airflow	cond	Fourier conduction
Pr	Prandtl number	lam	laminar
P	pressure	m,Le	mass transfer based on analogy
t	time	m,exp	mass transfer from experiment
T	temperature	roof	roof materials
q	heat flux	s	exterior roof surface
R	ratio $\left(h_{m,exp}/h_{m,Le}\right)$	sat	saturated
Re	Re number	sen	sensible heat gain
Sc	Schmidt number	sky	radiant sky
Nu	Nusselt number	turb	turbulent
Sh	Sherwood number	wv	water vapor
Le	Lewis number	**Superscript**	
Fo	Fourier number	$\overline{}$	average or partial pressure
ω	specific humidity	1	new value at time t +Δt
ϕ	relative humidity	0	present value at time t
ε	total infrared emittance	*	previous iteration value

ANALOGY BETWEEN HEAT AND MASS TRANSFER

Air flow across a flat plate will develop thermal and concentration boundary layers. Scaling the convective energy and species equations and their respective boundary conditions results in the following set of dimensionless equations:

$$\overline{u}\frac{\partial\overline{T}}{\partial\overline{x}}+\overline{v}\frac{\partial\overline{T}}{\partial\overline{z}}=\frac{1}{\left(Re_L\right)Pr}\frac{\partial^2\overline{T}}{\partial\overline{z}^2} \qquad \underbrace{\overline{T}(\overline{x},0)=0}_{\text{Wall Boundary Condition}}\ ,\quad \underbrace{\overline{T}(\overline{x},\infty)=1}_{\text{Free Stream Boundary Condition}} \tag{1}$$

$$\bar{u}\frac{\partial \bar{C}_a}{\partial \bar{x}} + \bar{v}\frac{\partial \bar{C}_a}{\partial \bar{z}} = \frac{1}{(Re_L)Sc}\frac{\partial^2 \bar{C}_a}{\partial \bar{z}^2} \qquad \underbrace{\bar{C}_a(\bar{x},0) = 0}_{\substack{\text{Wall}\\ \text{Boundary Condition}}}, \quad \underbrace{\bar{C}_a(\bar{x},\infty) = 1}_{\substack{\text{Free Stream}\\ \text{Boundary Condition}}} \tag{2}$$

Because the equations and boundary conditions are of the same dimensionless form, the convective heat and mass transfer processes are analogous. That is, the dimensionless relations that drive the thermal boundary layer are the same as those that drive the concentration-boundary layer. Advection to the flat plate is governed by the Re number; diffusion is characterized by the Pr number [Eq. (1)] and by the Sc number [Eq. (2)]. The definitions for heat transfer $Nu = a(Re_L)^b(Pr)^c$ and for mass transfer $Sh = a(Re_L)^b(Sc)^c$ can therefore be combined and reduced to the following form:

$$\frac{\hbar_L}{\bar{h}_m(\bar{\rho}\cdot C_P)_{air}} = \left(\frac{\alpha}{D_{ab}}\right)_{air}^{1-c} \tag{3}$$

The result is known as the analogy between heat and mass transfer and is applicable to both laminar and turbulent flows. The relation is also valid for free convection. The ratio α/D_{ab} is defined as the Le number, which describes simultaneous heat and mass transfer by convention. Kusuda (1965) recommends that c = 1/3 so that the Le number is raised to the 2/3 power for forced-convection flow. Moist air properties yield an Le number of about 0.85, and the right-hand side of Eq. (3) would therefore be about 0.9, close to unity. Given a correlation for the heat-transfer coefficient, one can easily calculate the mass-transfer coefficient. Hence, the approach is very useful because of the multiplicity of heat-transfer correlations in the open literature and because of the dearth of mass-transfer correlations for moist-air dehumidification.

Shah (1981) showed that the analogy for heat and mass transfer is reliable provided the airflow is fully turbulent and exceeds 5.6 mph (2.5 m/s) at any air-to-water temperature difference. At lower airflow rates, the analogy is accurate provided the air-to-water temperature gradient exceeds about 27F° (15C°). Unfortunately, during the late twilight hours of any summer day, both the roof-to-air temperature gradient and the wind speed are usually below these limits. Shah (1981) checked the predictive accuracy of mass-transfer algorithms formulated by Carrier (1918), by Meyer (1915), and by the classical analogy between heat and mass transfer. He recommends the Carrier equation at low velocities and the analogy at higher velocities. However, for plate-to-ambient temperature gradients less than 27F° (15C°) Shah could not substantiate the accuracy of the analogy. A study was therefore conducted to correlate mass transfer occurring at low velocities and at low-temperature gradients, which occur more often than not on a low-slope roof.

LITERATURE CORRELATIONS FOR DEHUMIDIFICATION

Nusselt and Sparrow (1916), Minkowycz and Saddy (1967), and numerous others have studied the dehumidification of moist air onto a flat plate and have verified and documented the analogy between heat and mass transfer. Varma, Charan, and Soogappa (1978) studied the simultaneous transfer of heat and mass from moist air condensing on a flat plate held at subfreezing temperatures. The mass-transfer coefficient was predicted using Eq. (3) and compared to their measured data. The analogy was a factor of 3 less than their experimental data! Varma, Charan, and Soogappa (1978) formulated a correlation based on the moist air enthalpy potential, the specific humidity gradient from the air to the plate, and the Re number. The correlation agreed within ±20% of their experimental data. Their formulation is multiplicative in form and is applied as a factor to the heat- and mass-transfer analogy as follows:

$$\frac{h_{m,exp}}{h_{m,Le}} = 53{,}500\left(\frac{i_{air} - i_s}{i_{fg}}\right)^{1.2}\left(\frac{\omega_{air} - \omega_s}{Re}\right)^{0.3} \tag{4}$$

The experiments conducted by Varma, Charan, and Soogappa (1978) had temperature gradients from the moist air to the plate greater than 27F° (15C°); the velocity did not exceed 5.6 mph (2.5 m/s). Although they

studied the advection of moist air under frosting conditions, their results show strong evidence for potential improvement in the heat-and-mass-transfer analogy, especially in the laminar flow regime.

Yaghoubi, Kazeminejad, and Farshidiyanfar (1993) analytically studied the heat and mass transfer from dry and humid air flowing over a flat plate. A correlation was derived from their numerical results, which showed the heat transfer for humid air was significantly different from that of dry air. Yaghoubi, Kazeminejad, and Farshidiyanfar (1993) observed the Nu number increased with increases in the relative humidity of the ambient air and with reductions in the barometric pressure. They also observed that the Nu number increased with an increase in the difference of the partial pressure of humid air to that saturated at the plate surface. They correlated an expression for the local, sensible $Nu_{x,sen}$ number of the form:

$$Nu_{x,sen} = \frac{0.902\,Re^{0.5}\left(\dfrac{\overline{P}_{WV} - \overline{P}_{sat}}{P_{atm}}\right)^{0.524}\phi^{0.177}}{\left(\overline{P}_{WV}/P_{atm}\right)^{0.337}} \tag{5}$$

Yaghoubi, Kazeminejad, and Farshidiyanfar (1993) validated their correlation against the experimental data of Legay-Desesquelles and Prunet-Foch (1986); it is applicable in both laminar and turbulent flow regimes for $\phi > 50\%$ relative humidity.

ROOF ENERGY BALANCE

An energy balance at the exterior surface of the roof (Figure 1) is needed to mathematically describe the boundary condition for the heat flow through the roof. The convection ($\hbar$), the mass transfer (h_m), and the surface properties of reflectance (ρ) and emittance (ε) affect the exterior temperature and, therefore, the heat flow in the following equation:

$$\begin{aligned} q_{cond} &= q_{roof} \\ -k\left(\frac{dT}{dz}\right)_S &= (1-\rho)I_{solar} - \varepsilon\sigma\left(T_S^4 - T_{sky}^4\right) - \hbar_L\left(T_S - T_{air}\right) + \overline{h}_m i_{fg}\left(\omega_{air} - \omega_S\right) \end{aligned} \tag{6}$$

The equation is nonlinear because of the radiation and mass transfer energy terms. A numerical scheme is therefore required to solve for the temperature and heat-flow profiles through the roof. Wilkes (1989) formulated a code after the discretization techniques presented by Patankar (1984). The code, termed STAR[2], models the transient one-dimensional heat flow through the exterior roof cover, through multiple layers of roof insulation, and through the supporting sub-frame (e.g., a metal deck). The energy equation in time and one-dimensional space is linearized into a collection of simultaneous algebraic equations. The equations are fully implicit and mathematically describe the temperature for a given time and position within the multi-layer roof. A numerical solution of the algebraic equations leads to the temperature profile throughout the roof insulation from which the heat leakage of the building is calculated using Fourier conduction.

Discretization

To model the exterior boundary condition (Figure 1), the energy equation is integrated over small increments of time and space into the roof as follows:

$$\int_b^s \int_t^{t+\Delta t} \left(\overline{\rho}\cdot C_P\right)_{roof} \frac{\partial T}{\partial t}\,dt\,dz = \int_b^s \int_t^{t+\Delta t} \frac{\partial}{\partial z}\left(k\frac{\partial T}{\partial z}\right)dt\,dz \tag{7}$$

[2] **Simplified Transient Analysis of Roofs.**

The integration leads to the following balance:

$$\left(\bar{\rho}\cdot C_P\right)_{roof}\left\{T_S^1 - T_S^0\right\}\frac{\Delta z}{2} = \int_t^{t+\Delta t}\left\{\left(k\frac{\partial T}{\partial z}\right)_S - \left(k\frac{\partial T}{\partial z}\right)_b\right\}dt \tag{8}$$

The flux term $k\left(\partial T/\partial Z\right)_S$ represents the heat flux at the roof surface (q_{roof}). Substituting the right-hand side of Eq. (6) into Eq. (8) accounts for the effects of the outdoor ambient weather. Taylor series expansions are applied to the radiation and mass-transfer terms to approximate them in linear formulations, and Eq. (8) is integrated from time t to time t + Δt. The resultant, fully implicit equation becomes:

$$A_S T_S = A_b T_b + B \tag{9}$$

where

$$A_S = \left\{A_S^0 + 4\varepsilon\sigma T_S^{*3} + \bar{h}_m i_{fg}\frac{d\omega_S^*}{dT} + \hbar_L + \frac{k_b}{\partial z_b}\right\}$$

$$A_b = \frac{k_b}{\partial z_b}$$

$$A_S^0 = \left(\bar{\rho}\cdot C_P\right)_{roof}\frac{\Delta z}{2\Delta t}$$

$$B = (1-\rho)I_{solar} + \varepsilon\sigma\left(T_{sky}^4 + 3T_S^{*3}\right) + \bar{h}_m i_{fg}\left\{\omega_{air} - \omega_S^* + \frac{d\omega_S^*}{dT}T_S^*\right\} + \hbar_L T_{air} + A_S^0 T_S^0$$

Wilkes (1989) compiled an extensive literature review of convective-heat-transfer correlations for natural and forced convection. His compilation of correlations accounts for the effects of heat-flow direction, surface orientation, surface area, and advection. The STAR code selects the appropriate correlation based on roof slope and also on the direction of heat flow. For laminar flow, the local heat-transfer coefficient is derived from the similarity solution of the Blasius equation [in honor of H. Blasius (1908)]. The coefficient takes the following form:

$$\frac{h_x x}{k} = 0.332\,Re_x^{1/2}\,Pr^{1/3} \tag{10}$$

In turbulent flow, the boundary layer over a flat plate is affected more by random fluid fluctuations than by molecular diffusion (Incropera and DeWitt 1990). The momentum, thermal, and concentration boundary layers are essentially equal for moist air having a Pr number near unity. The heat-transfer coefficient can therefore be derived from the Chilton-Colburn analogy (i.e., Reynolds analogy). Thus, from the experiments by Schlichting (1968), who formulated a solution for the velocity-boundary-layer thickness, and by the Reynolds analogy relating momentum to heat transfer, the local heat-transfer coefficient for turbulent flow becomes

$$\frac{h_x x}{k} = 0.0296\,Re_x^{4/5}\,Pr^{1/3} \tag{11}$$

Typically, a transition from laminar to turbulent flow occurs sufficiently upstream of the rear edge of the flat plate [i.e., low-slope roof ≅ 36 ft (11 m) long in direction of airflow]. Integrating the local laminar and turbulent coefficients over their respective domains by the following formula

$$\hbar_L = \frac{1}{L}\left\{\int_0^{x_C} h_{lam}\,dx + \int_{x_C}^{L} h_{turb}\,dx\right\} \tag{12}$$

yields the overall average heat-transfer coefficient for a $Re_{x,C} = 500{,}000$:

$$\frac{\hbar_L L}{k} = \left\{0.37\,Re_L^{4/5} - 871\right\}Pr^{1/3} \tag{13}$$

The STAR code uses Churchill's technique to combine the natural-convection flows, which occur primarily during the daylight hours, with forced-convection flows (Churchill 1986). Given this formulation for the combined natural- and forced-convection coefficient ($\hbar_L$), the mass transfer is directly calculated from the Le number [Eq. (3)]. The model also uses ambient weather[3] data to complete the physics of the problem. The dry bulb temperature, relative humidity, and barometric pressure are used to calculate the specific humidity of the ambient air. The radiant-sky temperature is derived from the global infrared irradiance measured by the Buildings Technology Center's (BTC's) field pyrgeometer and the equation for blackbody radiation: $q_{IR} = \sigma T_{sky}^4$. If pyrgeometer data are unavailable, STAR uses the Martin and Berdahl (1984) algorithm to calculate the radiant-sky temperature.

EXPERIMENTAL FACILITY

Several metal roofing associations and the Single-Ply Roofing Institute (SPRI) are conducting three-year cooperative research projects at the BTC to determine the effects of a roof's solar reflectance and infrared emittance on building cooling and heating requirements. SPRI and the consortia of metal industries are conducting their studies on ORNL's Envelope Systems Research Apparatus (ESRA), which resembles a residential basement topped with a typical commercial low-slope roof (Figure 2).

While validating the STAR code against the ESRA field data, investigations revealed the mass transfer to the roof was underpredicted. Therefore, a study was conducted to improve the mass-transfer algorithm in parallel to the field study to better predict the roof temperature and the heat transfer through the roof. Experimental data collected from the field tests were used to help formulate and validate the mass-transfer correlation.

SPRI Low-Slope Test Assembly

The ESRA's low-slope assembly consists of steel joists and bridging that support a metal deck made of 22-gage, 0.030-in.- (0.76-mm-) thick galvanized steel. The deck's ribbing is narrow, about 1 1/2 in. (38.1 mm) wide. Wood fiberboard, 1 in. (25.4 mm) thick, lies atop the deck, and a thinner 1/2-in.- (12.7-mm-) thick piece of wood fiberboard is placed atop the 1 in. (25.4 mm) layer. The low-slope metal roofs and single-ply membranes are attached using standard fastening practice and cover the 1 1/2 in. (38.1 mm) of fiberboard insulation.

Instrumentation

Each test lane (Figure 2) is instrumented with copper-constantan thermocouples for measuring the temperature gradients across the roof insulation (Figure 3). The thermocouples are placed in the ESRA's indoor ambient, attached to the bottom side of the membrane, taped between the two layers of fiberboard, and placed atop the surface of the 1/2-in.-thick (12.7 mm) piece of wood fiberboard. A 2-in.-square (50.4 mm) by 0.18-in.-deep slot (4.6 mm) was routed into the top of the 1-in. (25.4-mm) wood fiberboard so that a heat-flux transducer (HFT) could be placed there. All transducers were calibrated before being installed into the low-slope assembly. Each HFT was calibrated by being placed in a 12- by 12-in. (0.305- by 0.305-m) guard made from the same lot of wood fiberboard as that used in construction of the low-slope assembly. The sandwich of 1/2-in.-thick

---

[3] **The BTC monitors and electronically records ambient air temperature, relative humidity, barometric pressure, wind speed and wind direction, incident global solar radiation as measured on a horizontal surface, and infrared radiation over the 4- to 50-μm wavelength.**

(12.7 mm) wood fiberboard, the HFT, and 1-in.-thick (25.4 mm) wood fiberboard was placed in a heat-flow meter calibration apparatus to develop a calibration that corrects for edge effects. The HFT manufacturer states accuracy as ±1% of full-scale reading with a sensitivity of about 1.3 Btu/(h · ft^2) per mv of signal (4.1 W/m^2 per mv). Our calibrations showed them to be accurate within ±5% of reading.

RESULTS

Data for the week of September 3–9, 1999, were selected for formulating and validating a correlation to augment the analogy for mass transfer occurring at low Re number and at low ambient air-to-membrane temperature gradients. This particular week was selected because, on the evening of September 8 and the morning of the 9th, the membrane temperature of the test roofs exceeded the dew point temperature of the ambient air, and the roofs were dry. Weather conditions in east Tennessee seldom produce dry air. However, for those two particular periods, the ESRA roof was dry. We observed a close match between the predicted and the measured temperature of several of the single-ply membranes over the early morning hours. On evenings when dew formed on the test roofs, the STAR code underpredicted the measured membrane temperature by as much as 3F° (1.7C°).

Data of the air-to-membrane temperature gradient measured for the test roofs as well as the wind speed measured across the ESRA help reveal the uncertainties in accurately predicting the mass transfer (Figure 4)[4]. From about 8 P.M. until 8 A.M. on these mild summer nights, the membrane is colder than the ambient air. However, the maximum temperature difference does not exceed 10F° (5.6C°), well below the limit for using the heat-and-mass-transfer analogy to reliably predict the mass transfer as recommended by Shah (1981). Further, the wind speed is less than 2 mph (0.89 m/s); therefore, the Re number is less than 500,000, and the measured airflow is laminar, again below the limit stated by Shah (1981).

During the evening hours, the convective heat-transfer coefficient is driven primarily by forced-convection flow. Natural convection is low because the air-to-membrane temperature gradient is less than about 10F° (5.6C°) (Figure 4). The solid line in Figure 5 therefore represents forced-convection heat transfer that occurs from about 8 P.M. to 8 A.M. for the days of September 3–8, 1999; Septemper 9 had some mild winds. The change in slope of the solid curve occurs as the heat transfer transitions from laminar to turbulent[5] flow at Re numbers exceeding 500,000 (Figure 5). The coefficient is largest around solar noon (Figure 6). At night, as the roof cools and any ambient air turbulence settles, the coefficient decreases to its lowest value (Figure 6), it being only about 0.2 Btu/(h·ft^2·°F) [1.1 W/(m^2·°C)]. Solar irradiance increases as the sun reaches solar noon, and the membrane temperature exceeds the air temperature by about 40F° (22.2C°), warming the air within the boundary layer, which in turn increases the buoyancy forces atop the roof. Convection-heat transfer becomes a mix of forced- and natural-convection forces (data above forced convention curves in Figure 5). Hence, because of the additional component of natural convection, data for the heat-transfer coefficients occurring around solar noon exceed those observed at night and are seen above the solid curves in Figure 5 as mixed-convection heat transfer.

Mass Transfer

Mass transfer occurs on the roof from about 8 P.M. to 8 A.M., when the membrane temperature drops below the dew point temperature of the ambient air. During these evening hours, the convective-heat transfer is based almost solely on the wind flowing across the ESRA, and the mass-transfer coefficient is derived from Eq. (3) using the convective-heat-transfer correlations given in Eqs. 10 and 13 (i.e., represented by the solid curves in Figure 5).

We compared the mass transfer calculated from the analogy to that back-calculated from temperature measurements on the ESRA roof. The STAR code was run using the exterior membrane temperature and the deck temperature as boundary conditions to eliminate the uncertainties of weather. The code calculated the heat flux at the membrane using Fourier conduction, and the mass transfer was back-calculated from this exterior flux using Eq. (6). The results in Figure 7a reveal that, as condensation begins, the actual mass transfer is significantly higher than that calculated by the analogy. Inspection of Figure 4 shows the largest air-to-membrane temperature gradients occur for roughly 1 h past the start of condensation. Both the energy exchange from the mass transfer and the accumulation of liquid atop the roof cause the temperature gradient to drop

---

[4] **The labels on the abscissa in Figures 4, 6, and 9 represent midnight for each consecutive day.**

[5] **A turbulent flow driven by a mild wind was observed during the early hours of September 9 (Figure 4).**

(Figure 4). The mass transfer therefore drops and tends to follow the analogy (Figure 7a). The ratio of the back-calculated mass to the mass transfer based on the analogy shows a significant enhancement where gradients are largest. However, the ratio exponentially decays to 1 within about 3 h (Figure 7b). Obviously, overall coefficients do not account for the transients observed as humid air condenses onto the roof.

The Correlation

A correlation was formulated that supports the analogy by better capturing the transients at the start of condensation. A scaling of the energy equation for transient heat flow leads to the dimensionless time variable, the Fo number: $Fo = \alpha_{air} t / L^2$. Here we use the Fo number to compare the thermal diffusion from humid air to the length of the roof. The thermal diffusivity is based on the properties of saturated moist air evaluated at the average of the membrane and ambient air temperatures. The time in the Fo number was selected to be that time associated with the start of condensation.

Varma, Charan, and Soogappa (1978) as well as Yaghoubi, Kazeminejad, and Farshidiyanfar (1993) each formulated their correlation in terms of the Re number and moist-air gradients evaluated from the ambient air to the plate (see Eqs. 4 and 5). However, regression analysis showed best fit using humid-air potentials rather than gradients. Because the potentials are a function of the ambient air and not the exterior roof temperature, the numerical procedure will also be more stable in calculating a convergent solution. The correlation fit takes the form

$$R \equiv \frac{h_{m,exp}}{h_{m,Le}} = C_1 \, Re_L^{C_2} \, Fo_L^{C_3} \left(\frac{\overline{P}_{WV}}{P_{atm}} \right)^{C_4} \tag{14}$$

where

	C_1	C_2	C_3	C_4
for $Fo \le 0.0009$	9,529.0	-1.716	-1.250	-1.237
for $Fo > 0.0009$	13,568.4	-1.683	-0.189	-2.889

The multiplicative factor (R) is applied directly to the analogy between heat and mass transfer [Eq. (3)]. It is superimposed on field measurements collected on the 7th and 8th of September when water vapor condensed onto the ESRA roofs (Figure 7b). As time progresses past the start of condensation, the factor reduces to the analogy. Best fit to the data occurred if the correlation was grouped by the strength of the Fo number; the adjusted RMS[6] error for the fit is 0.72.

The results of correlating the data are also shown in Figure 8a where the experimental data are scaled by the normalizing variable: $NV_1 = Fo_L^{C_3} \left(\overline{P}_{WV} / P_{atm} \right)^{C_4}$. The two curves in Fig 8a represent the correlation by the form $C_1 \, Re_L^{C_2}$ and are superimposed onto the scaled data to compare the correlation to the reduced data. Given the uncertainty in mass-transfer measurements, the correlation does a good job of describing the data. Analysis showed that increasing the Re number from laminar to turbulent flow should reduce the factor toward 1 because the analogy is accurate for turbulent flows. Varma, Charan, and Soogappa (1978) found a similar dependence on the Re number. The negative coefficient on the ratio of the partial pressure of water vapor in air to the atmospheric pressure $\left(\overline{P}_{WV} / P_{atm} \right)$ is consistent with that derived by Yaghoubi, Kazeminejad, and Farshidiyanfar (1993). As the partial pressure of water vapor in air increases, the dew point and dry bulb temperature must increase and the air-to-plate temperature potential increases toward the recommended temperature gradients stated by Shah (1981). Also, reducing the humid-air atmospheric pressure enhances the mass transfer (Yaghoubi, Kazeminejad, and Farshidiyanfar 1993).

---

[6] RMS is the root mean square error and refers to the proportion of the total variation about the mean explained by the correlation.

A point-by-point review of the error incurred by the correlation is shown in Figure 8b. The ordinate is the correlation scaled by the experimental data. Therefore, data falling onto the graph at an ordinate value of 1 have perfect agreement. Those above 1 are overpredicted by the correlation; those below are underpredicted. For all the data, the average absolute error is about 30% of the experimental measure. For the uncertainty in mass- and heat-transfer coefficients, which can easily be as high as ±50%, the correlation predicts the experimental data very well (see also Figure 7b).

Validations

The correlation was programmed into the STAR code, and simulations were run for the week September 3–9, 1999 (data displayed in Figures 4 through 7). The analogy for heat and mass transfer causes the simulated membrane temperature to be underpredicted by as much as 3F° (1.7C°) during the evening hours for each weeknight displayed in Figure 9a, except on the evening of September 8th and the early morning of the 9th. Atmospheric conditions caused the roof to remain dry, and it was this observation that led to the formulation for the mass-transfer correlation.

The correlation causes the simulated membrane temperature to better follow the measured data during times of condensation (Figure 9). The average predictive error is about 4% of the measured membrane temperature for the whole week of data (Figure 9a). As a result, the heat flux simulated by STAR does a better job in predicting the heat leakage from the roof during the evening hours. Previously, the simulation overpredicted the heat leakage because the analogy underpredicted the mass transfer. Using the correlation to support the analogy, the error in the total heat flow through the roof, integrated over the week of data for September 3–9, 1999, is about 5% of the experimental measurement as compared to 25% when using only the analogy (Figure 9b).

CONCLUSIONS

A correlation for mass transfer onto a low-slope roof was formulated and validated against extensive experimental data. The correlation provides a simple and direct enhancement to the analogy for heat and mass transfer. It captures the transient effects at the onset of condensation and is applicable to laminar, low-temperature-gradient, mass-transfer phenomena, which frequently occur atop low-slope roofs.

Regression analysis showed the experimental data had a strong dependence on the Re number, the Fo number, and the ratio of the partial pressure of water vapor in air to the atmospheric pressure. The regression equation explains 72% of the total variation in the data. The average absolute error in the correlation's prediction is about 30% of the experimental measure.

The correlation causes the simulated membrane temperature and, therefore, the simulated heat flux to better follow the measured data during the times when humid air condenses onto a roof. The average predictive error in the membrane temperature is about 4% of the measured temperature. Using the correlation to support the analogy, the cumulative error over all hours in the heat flow through the roof is about 5% of the experimental measurement.

REFERENCES

Baker, M. C. 1980. *Roofs*. Polyscience Publications Inc., Montreal, Quebec, Canada.

Blasius, H. 1908. *Z. Math. Phys*, Vol. 56, pt. 1.

Carrier, W. H. 1918. "The Temperature of Evaporation." *Transactions of ASHVE*, Vol. 24, 25–50.

Churchill, S. W. 1986. "Mixed Convection Heat Transfer." *J. Heat Transfer*, Vol. 108, 835–840.

Incropera, F. P., DeWitt, D. P. 1990. *Fundamentals of Heat and Mass Transfer*. 3rd ed. John Wiley & Sons, New York.

Kusuda, T. 1965. "Calculation of the Temperature of a Flat-Plate Wet Surface under Adiabatic Conditions with Respect to the Lewis Relation." in *Humidity and Moisture, Vol. 1: Principles and Methods of Measuring Humidity in Gases*, 16–32, Reinhold Publishing Corporation, New York.

Legay-Desesquelles, F., Prunet-Foch, B. 1986. "Heat and mass transfer with condensation in laminar and turbulent boundary layers along a flat plate." *Int. J. Heat Mass Transfer*, Vol. 29, 95–105.

Martin, M., Berdahl, P. H. 1984. "Characteristics of Infrared Sky Radiation in the United States." *Solar Energy*, Vol. 33, 321–336.

Meyer, A. F. 1915. "Computing Runoff from Rainfall and Other Physical Data." *Transactions ASCE*, Vol. 79, Paper No. 1348, 1056–1224.

Nusselt, W. 1916. “Die Oberflächenkondensation des Wasserdampfes” (German). Zeitschrift VDI 60:541–46.

Schlichting, H. 1960. *Boundary Layer Theory*. 4th ed. McGraw-Hill, New York.

Shah, M. M. 1981. “Estimation of Evaporation from Horizontal Surfaces.” *ASHRAE Trans.*, Vol. 87, pt. 1. 35–51.

Sparrow, E. M., Minkowycz, W. J., Saddy, M. 1967. “Forced convection condensation in the presence of non-condensable and interfacial resistance.” *Int. J. Heat Mass Transfer*, Vol. 10, 1829–1845.

Varma, H. K., Charan, V., Soogappa, P. 1978. “Simultaneous Heat and Mass Transfer to a Flat Plate in Humid Air Stream Under Frosting Conditions.” *Letters in Heat and Mass Transfer*, Vol. 5, 297–305.

Patankar, S. V. 1984. *Numerical Heat Transfer and Fluid Flow*. Hemisphere, New York.

Yaghoubi, M. A., Kazeminejad, H., Farshidiyanfar, A. 1993. “Heat and Mass Transfer with Dehumidification in Laminar Boundary Layer Flow Along a Cooled Flat Plate,” *J. Heat Transfer*, Vol. 115, 785–788.

Wilkes, K. E. 1989. *Model for Roof Thermal Performance.* ORNL/CON-274. Oak Ridge, TN, Oak Ridge National Laboratory.

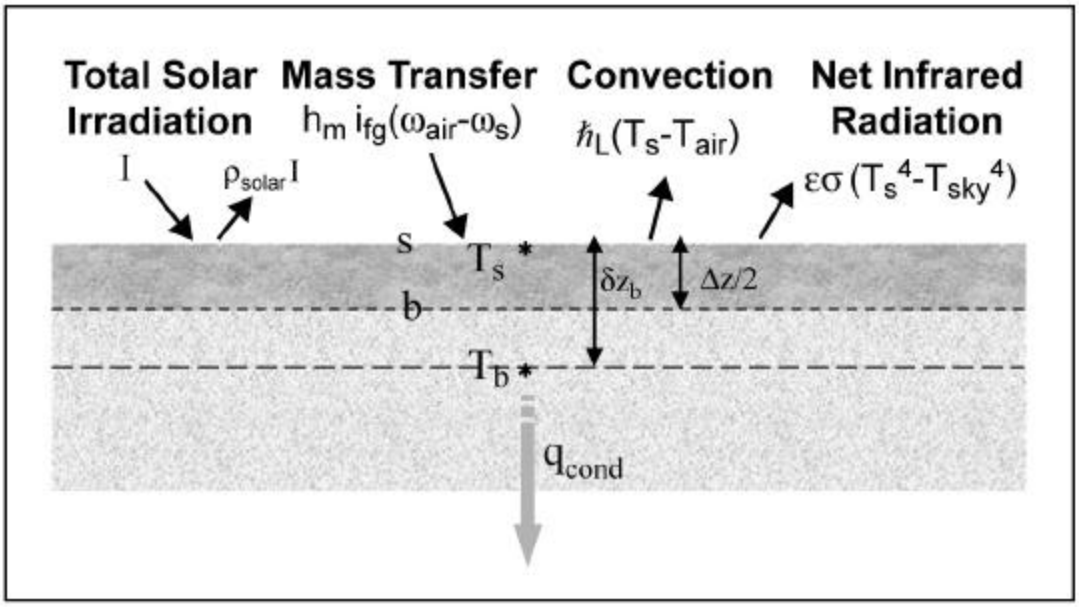

Fig. 1. Setup for integrating the roof energy balance into the numerical STAR computer code.

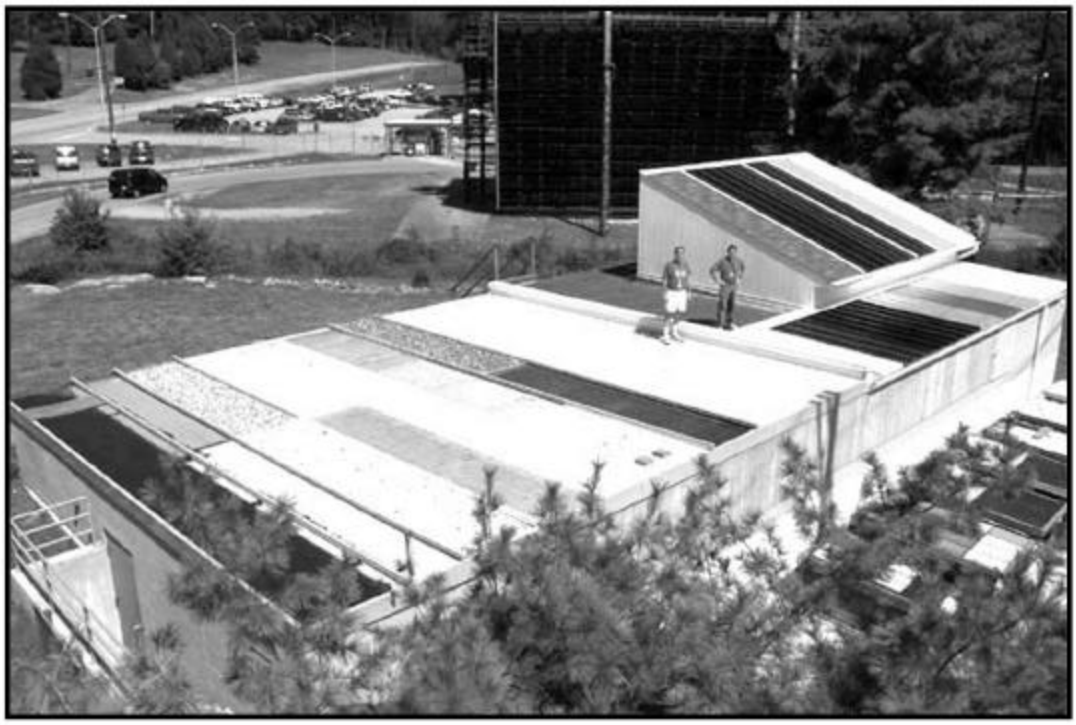

Fig. 2. The Envelope Systems Research Apparatus (ESRA) is used for conducting roof field exposure studies.

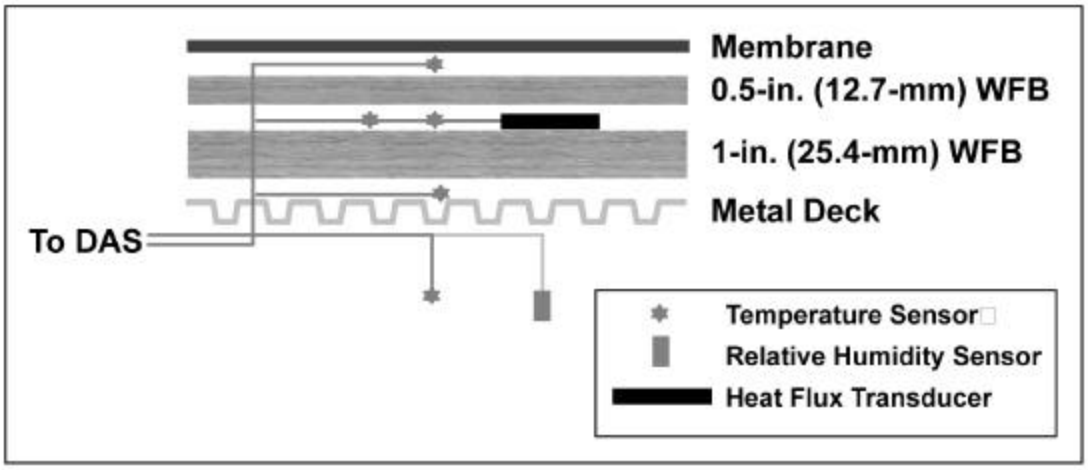

Fig. 3. Instruments are placed for measuring the temperature, heat flow and the ESRA indoor ambient temperature and relative humidity.

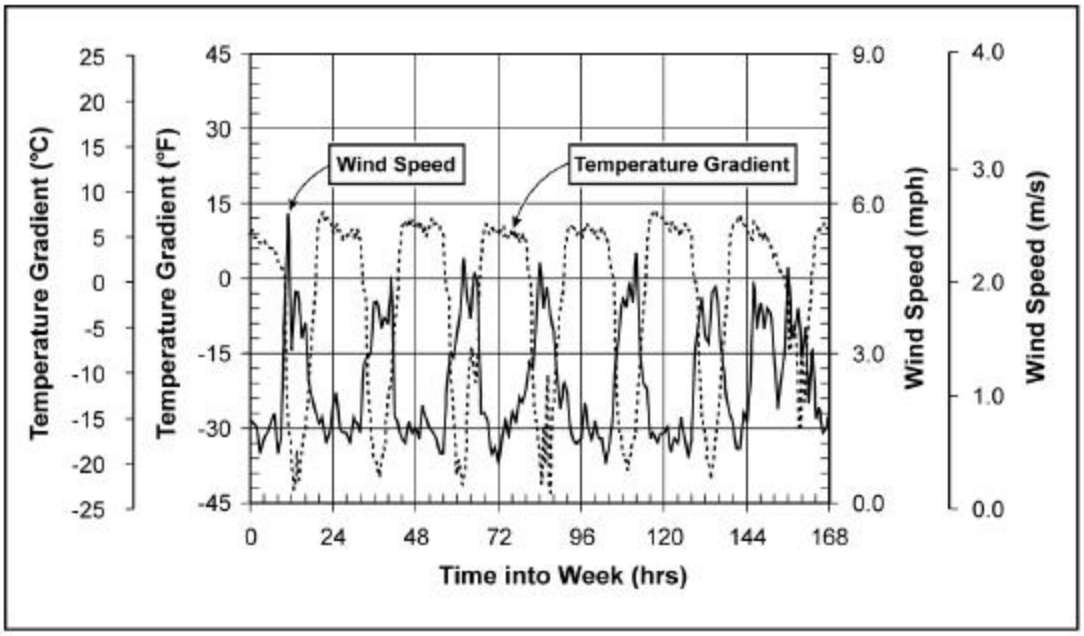

Fig. 4. The air-to-membrane temperature gradient and wind speed across the ESRA test roofs are monitored every 15-s and 15-min averages are recorded by the data acquisition system.

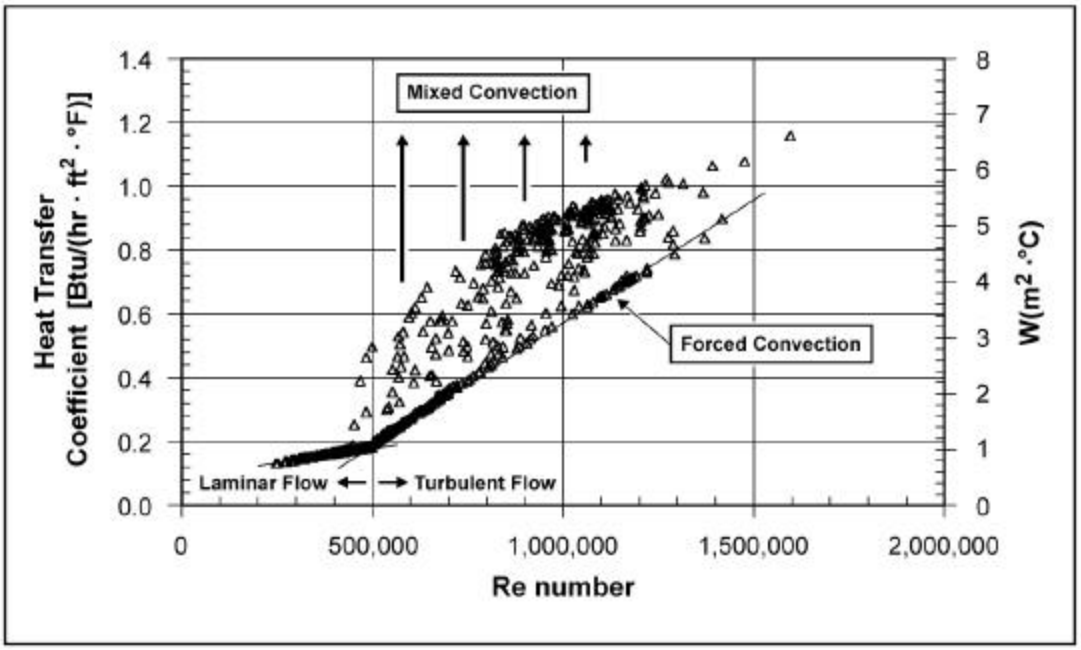

Fig. 5. Overall average convective heat transfer coefficient is calculated from the wind speed, the surface temperature and the outdoor ambient weather.

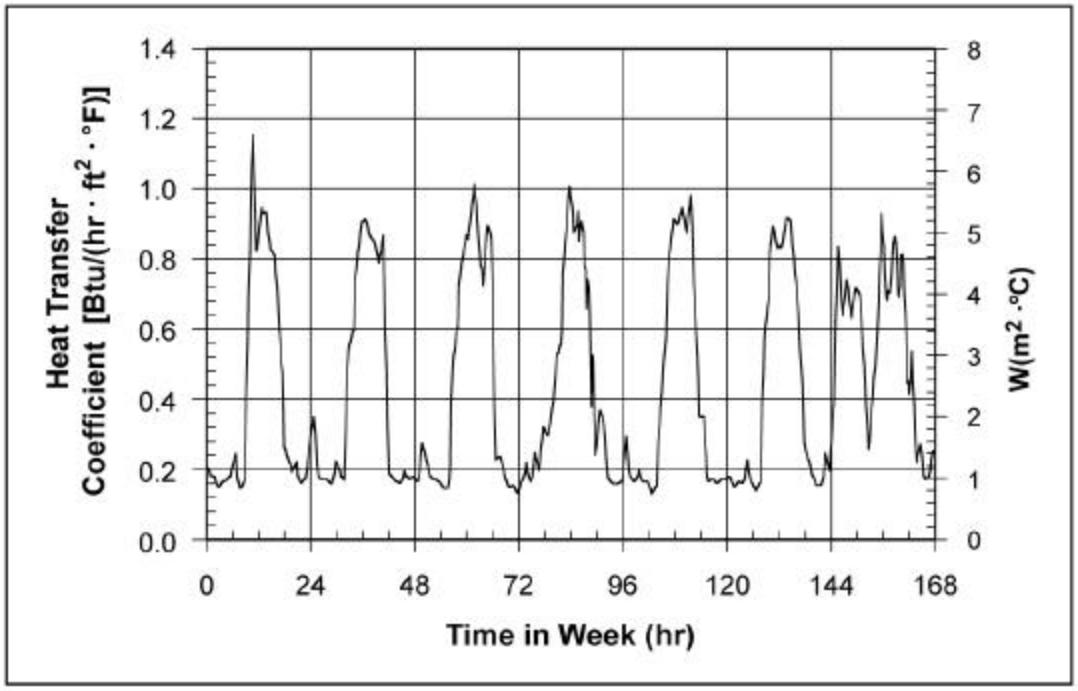

Fig. 6. The overall convective heat transfer coefficient is largest at solar noon and includes the effects of natural convection.

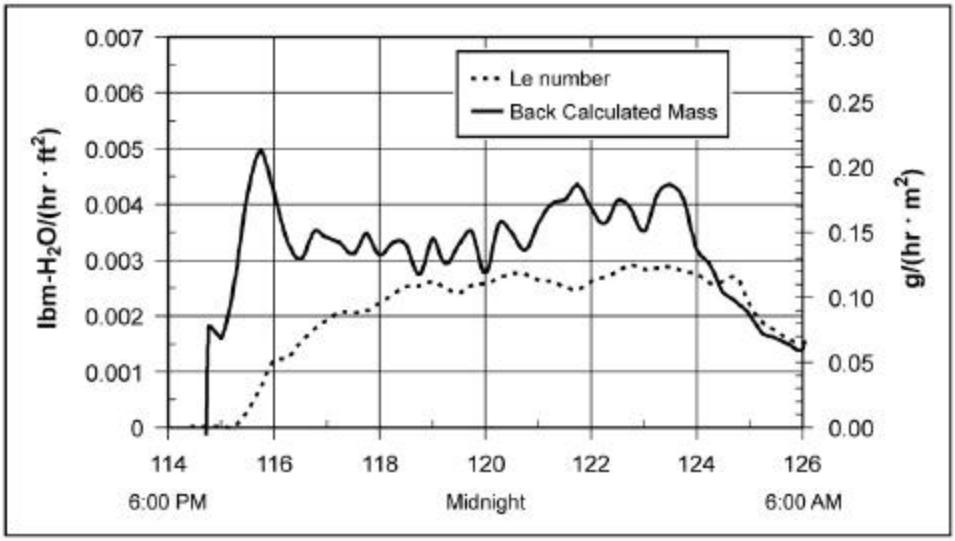

Fig. 7a. Mass transfer by the analogy is compared to the experimental value.

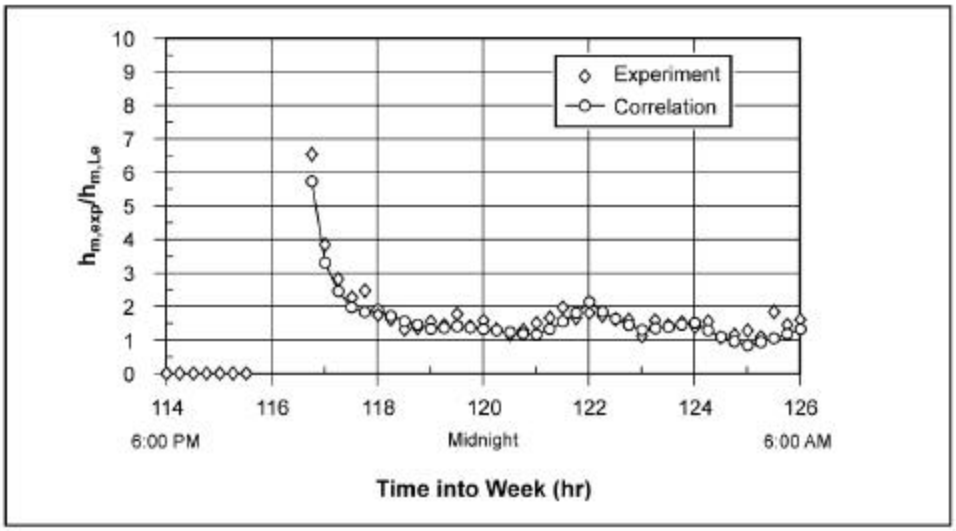

Fig. 7b. Correlation for mass transfer is compared to the experimental value.

Fig. 7. The mass transfer to the ESRA test roofs for the week of Sep. 3 — 9, 1999.

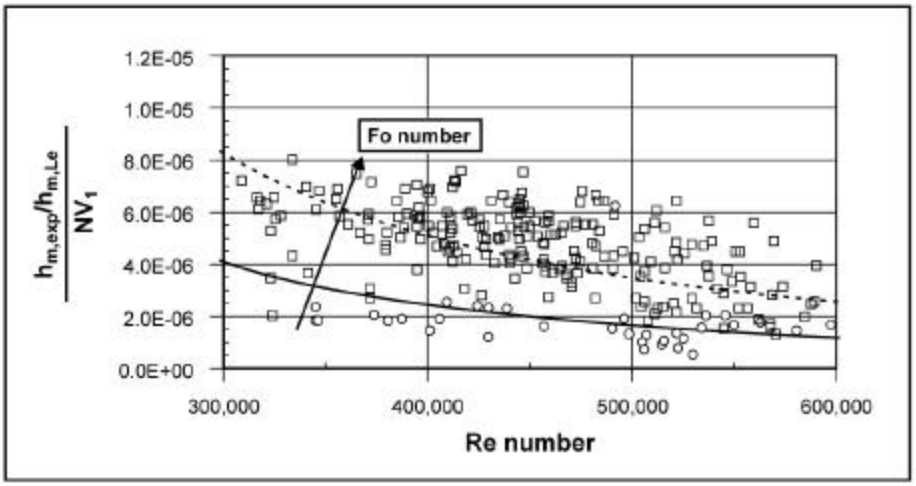

Fig. 8a. The correlation is scaled by the factor $NV_1 = Fo^{C3} (\bar{P}_{wv}/P_{atm})^{C4}$

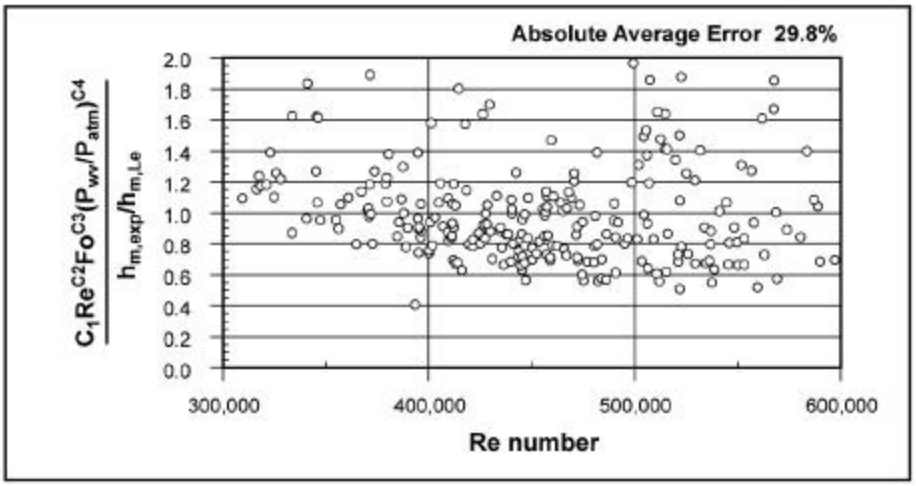

Fig. 8b. The correlation is scaled by the data to show the error.

Fig. 8. The goodness of fit of the correlation is scaled to compare it to the experimental measurements.

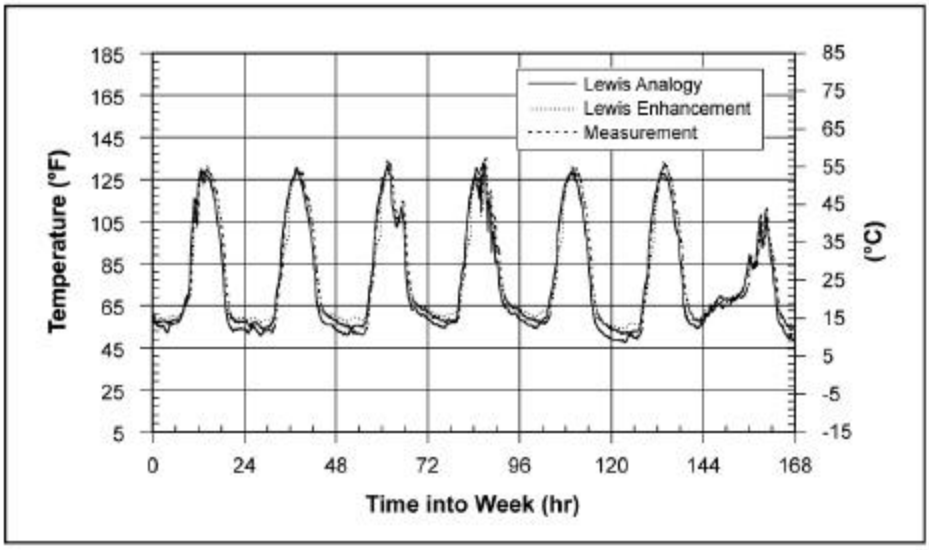

Fig. 9a. Comparison of the measurement and prediction for the membrane temperature.

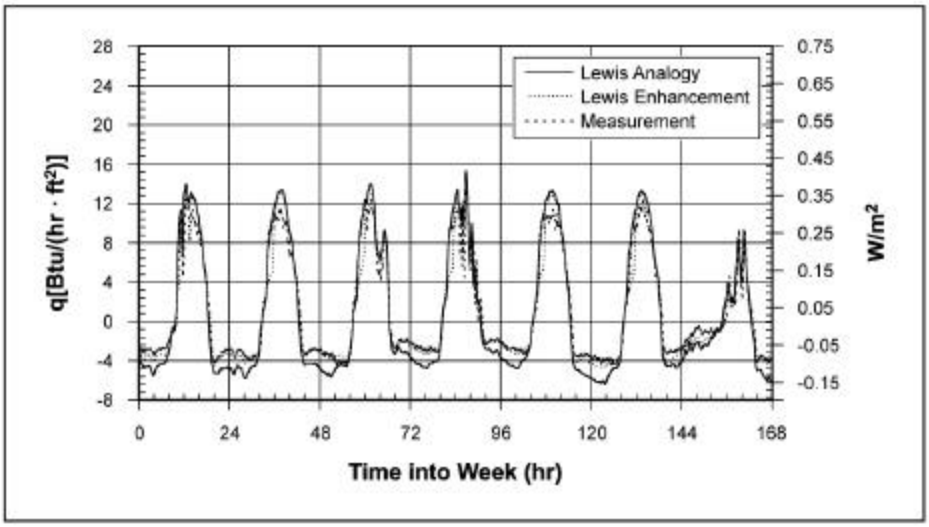

Fig. 9b. Comparison of the measurement and prediction for the heat flow.

Fig. 9. The correlation improves the STAR code's ability to predict the effects of mass transfer.